Transactions on Additive Manufacturing Meets Medicine
Trans. AMMM, 2026, Vol. 8, No 1, Article ID 2721, 11 Pages

Infinite Science Publishing

Original Research Article

Development of a parametric simulation framework for additively manufactured orthotic components considering patient-specific biomechanical requirements

T. Haupt*, S. F. Klimaschewski, M. Vehse, and N. Fuchs

Department of Mechanical Engineering, Hochschule Stralsund, Stralsund, Germany
** Corresponding author, email: torben.haupt@hochschule-stralsund.de*

Received March 2, 2026; **Accepted** April 21, 2026; **Published online** June 14, 2026

Abstract: The present study describes the development of a simulation-based model for the patient-specific design of functional orthotic components using additively manufactured spring structures. The aim of this study is to propose a methodology that facilitates the customization of functional, spring-like elements to individual biomechanical requirements. The design is executed parametrically, with geometric parameters systematically varied within a full factorial design of experiments. To represent the nonlinear and anisotropic behavior of additively manufactured polypropylene components in numerical simulations, the Three-Network-Model is employed and calibrated for the manufacturing orientations horizontal, diagonal, and vertical. The numerical analysis performed, utilizing the finite element method, facilitates precise prediction of force and moment responses over time under realistic loading conditions. The experimental validation demonstrated a high level of agreement with the simulation results, particularly for diagonally manufactured spring structures. Based on the finite element simulations, a quadratic regression model is developed for algorithmic geometry optimization and implemented in a semi-automated design tool. The utilization of patient-specific biomechanical data facilitates the design of orthotic components that are optimized both functionally and for manufacturing.

I. Introduction

Orthoses represent a pivotal component within the domain of orthopedic care, serving to stabilize, relieve, or correct impaired structures within the musculoskeletal system [1]. The orthotics market is experiencing continuous growth, driven in part by demographic change and the rising prevalence of chronic degenerative diseases. A market analysis indicates a steady increase in the orthopedic medical device segment, with sales projected to reach approximately 3.13 billion euros by 2025 and an expected annual growth rate of about 3.0 % until 2029 [2]. In the field of hand orthoses, the intricate anatomy of the hand and the numerous joints involved [3] impose stringent requirements on the accuracy of fit and the biomechanical efficacy of such devices [4]. Presently, orthotic care predominantly relies on prefabricated, off-the-shelf orthoses, which meet functional requirements but may exhibit limitations in terms of individual fit and wearing comfort. The impact of these limitations on patient compliance and therapeutic outcomes has been demonstrated to be negative [5]. Customized orthoses, by contrast, offer significant advantages in terms of biomechanical effectiveness, comfort and user acceptance due to their individual design. However, their conventional production requires considerable time and resources, which has so far limited widespread provision [6]. Advancements in the field of 3D-scanning technology have led to the development of cost-effective, high-resolution scanning devices that enable the capture of complex geometries with precision [7]. Concurrently, the manufacturing quality of additively manufactured components has undergone significant enhancement, thereby enabling the fabrication of complex human structures such as ears [7], teeth [8] or limps and the individual treatment of those structures with medical aids [9]. The use of simulation-based methods, particularly the finite element method (FEM), facilitates a realistic analysis and targeted adaptation to the (bio)mechanical behavior of the human body [10] and medical aids [11] prior to

manufacturing. This facilitates the optimization of dynamic elements, such as rotationally or flexural elastic structures, both geometrically and functionally, and their direct integration into the manufacturing process of the medical devices [11].

Against this background, the present study aims to develop and experimentally validate a numerical simulation and mathematical model for the patient-specific design of additively manufactured orthotic components. The focus is on the functional design of spring-like elements for the targeted transmission of forces during grasping. The main challenge lies in accurately representing the nonlinear material behavior of polypropylene, a material that is widely used in orthotics due to its biocompatibility and mechanical properties [12]. The analysis of the mechanical behavior of additive manufactured spring-elements is based on a full factorial design of experiments (DoE) that systematically varies geometric parameters of those functional orthotic elements [13]. Simulation validation is conducted through the mechanical testing of 3D-printed specimens under realistic boundary conditions.

In the long term, the developed model is intended to contribute to the digitized, efficient and functionally optimized production of patient-specific orthotics.

II. Material and methods

The selection of an appropriate material and methodological approach is crucial to the success of the research. Thermoplastic polymers such as polyamide (PA), acrylonitrile butadiene styrene (ABS), polyethylene (PE) and polypropylene (PP) are predominantly employed in the manufacture of hand orthoses [14]. In this study, polypropylene is used as it is well suited to the additive manufacturing process of Fused Filament Fabrication (FFF) and combines moderate stiffness with high elastic deformability. PP therefore fulfils the essential requirements for flexible yet dimensionally stable orthotic components. In addition, it exhibits high biocompatibility and low cytotoxicity. The Filament in use is the *P-Filament 721*, which is manufactured by *PPprint GmbH, Germany*. This Filament was certified in accordance with DIN EN ISO 10993-5 in 2023 [15].

II.I Parametric design of a spring geometry

At the initial stage of the research, a functional spring geometry is designed to form the basis of numerical simulations. This design is created using the computer aided design software *SolidWorks 2024* from *Dassault Systèmes, France*. The developed structure consists of an integrated spring element in the form of a parameterized tension spring. This parameterization is carried out via geometric characteristics to enable systematic variation of the geometry within the simulation framework. Attention is given to manufacturability via FFF, considering different layer orientations while printing and aiming for a design that is compact, comfortable and safe to wear. The parametric base design of the spring is shown in Fig. 1. The geometry is defined by the parameters: spring thickness (A), spring width (B), spring length (C) and pitch angle (D). The spring thickness is set at 2.5 mm, which corresponds to a conventional orthotic thickness that can be manufactured in a controlled manner in all three layer orientations, within limits of FFF [16]. The parameters B, C and D are directly transferred to the simulation environment to analyze different configurations within the framework of a DoE.

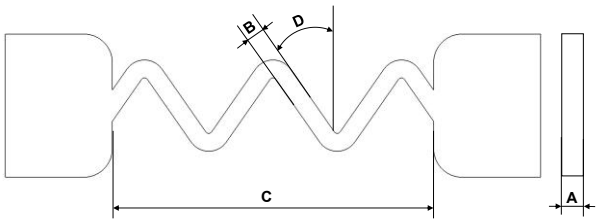

Figure 1: Parametrized spring geometry – thickness (A), width (B), length (C) and pitch angle (D)

To represent a realistic loading scenario, the spring geometry is modeled as an integral part of a surrogate specimen, see Fig. 2 (red). In the case of a hand orthosis, the spring element is positioned on the back of the hand and functions as a restoring mechanism or a means of transmitting force to the carpometacarpal (CMC) joint during grip movements. The process involves the use of finger force to extend the spring and thereby store energy. This extension occurs through rotation about the metacarpophalangeal joint II (MCP-II). The surrogate specimen incorporates an additional recess (a) for positioning the MCP-II joint, an extension of the lever arm (b) to initiate the rotation movement, and a defined clamping surface (c) for the measurement the resulting tensile force. This surrogate model is used in the finite element (FE) simulation and the experimental validation tests.

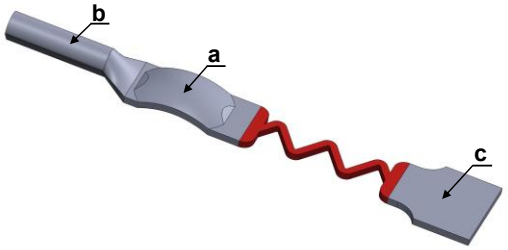

Figure 2: Surrogate specimen – spring element (red), recess (a), lever arm (b) and clamping surface (c)

II.II Full factorial design of experiments

The mechanical behavior of the spring component is systematically examined within the framework of a full factorial DoE. For this purpose, three geometric parameters: spring width, spring length and pitch angle are each divided into five discrete levels.

The complete combination of these levels yields a parameter space with a total of 5^3 (125) defined parameter

sets. Each parameter set corresponds to a unique geometric configuration that is analyzed by simulation regarding its mechanical performance.

The investigated parameter ranges are defined as follows: the spring width varies between 2.5 mm and 4.5 mm, the spring length between 45 mm and 65 mm, and the pitch angle between 35° and 55°. These values are based on experience gained from previous studies regarding manufacturability in FFF and applicability to dynamic orthotic components.

In addition to geometric variation, the influence of the build orientation is considered as a categorical factor. For this purpose, three typical layer orientations are examined: horizontal (0°), diagonal (45°), and vertical (90°) relative to the print bed. These correspond to the optimal component orientations in terms of manufacturing and resource efficiency and allow conclusions to be drawn about the anisotropic behavior of the spring component.

The evaluation of the DoE is performed using a quadratic regression model, which accounts for the main linear effects, the two-way interactions, and the squares of the effects of the three geometric parameters. The resulting equation, derived from the individual regression coefficients, can be used to predict one specific target variable.

Table 1: Material parameters used by the TNM [17]

Nr.	***Symbol***	***Description***
1	μ_A	Shear modulus of network A
2	$\widehat{\Theta}$	Temperature factor
3	λL	Locking stretch
4	κ	Bulk modulus
5	$\hat{\tau}_A$	Flow resistance of network A
6	a	Pressure dependence of flow
7	m_A	Stress exponential of network A
8	n	Temperature exponential
9	μ_{Bi}	Initial shear modulus of network B
10	μ_{Bf}	Final shear modulus of network B
11	β	Evolution rate of μB
12	$\hat{\tau}_B$	Flow resistance of network B
13	m_B	Stress exponential of network B
14	μ_C	Shear modulus of network C
15	q	Relative contribution of I_2 of network C
16	α	Thermal expansion coefficient
17	Θ_0	Thermal expansion reference temperature

II.III Material modelling of additively manufactured polypropylene

Polypropylene is a semi-crystalline thermoplastic which exhibits nonlinear deformation behavior. Due to its layered structure in additive manufacturing, it also develops anisotropic properties [18]. To consider, the properties mentioned above, it is necessary to use a nonlinear material model to simulate the mechanical behavior with the required degree of accuracy.

The Three-Network-Model (TNM), which has been specifically developed for thermoplastic polymers, is employed for the simulation [17]. The material parameters of the TNM are shown in Table 1. Previous studies have demonstrated the suitability of this model for modeling the mechanical behavior of PP [19]. The model is calibrated based on experimental data obtained from cyclic tensile tests. For this purpose, specimens of *type 1BA* are produced in accordance with *DIN EN ISO 527-2:2012-06.* Manufacturing is carried out using a *Prusa MK4* from *Prusa Research a.s., Czech Republic*. The specimens are printed in three building orientations. The tests are carried out in a total of nine load cycles, see Fig.3.

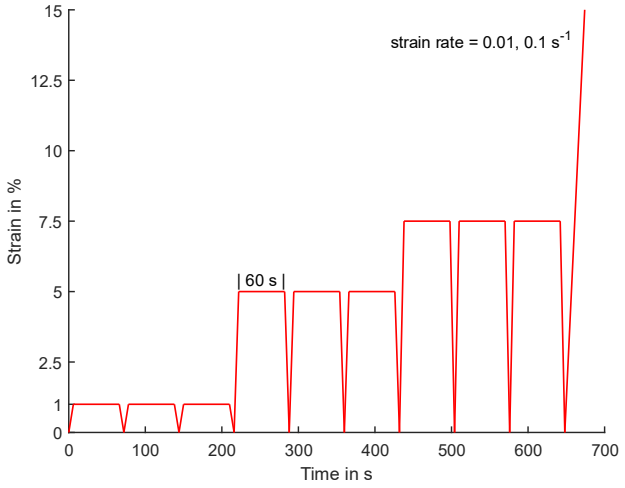

Figure 3: Schematic strain-time diagram of the tensile test sequence

At the point of maximum load, a holding time of 60 seconds is applied to capture the relaxation behavior. Subsequently, each specimen is loaded to failure or well into the region of plastic deformation to record the stress-strain behavior at failure. The corresponding manufacturing parameters are documented in Table 2. A separate material model is created for each of the three build orientations to account for the anisotropic properties. The initial calibration of the models is performed using *MCalibration* from *Ansys Inc., USA (formerly PolymerFEM, USA).* In this process, the TNM parameters are iteratively adjusted to minimize the deviation between the experimentally determined stress-strain behavior and the simulated results.

Infinite Science Publishing

Table 2: Manufacturing settings for additively manufactured test specimens

Nr.			Unit
1	3D-printer (FFF)	Prusa MK4	-
2	Filament	P-Filament 721	-
3	Extrusion temperature	210.00	°C
4	Print speed	10.00	mm/s
5	Print speed (overhangs)	7.50	mm/s
6	Layer height	0.15	mm
7	Bed temperature (1st layer / others)	70.00 / 20.00	°C
8	Fan speed	100.00	%
9	Infill	100.00	%
10	Nozzle diameter	0.40	mm
11	Perimeter count	6.00	-
12	Top/Bottom layers	none	-
13	Brim	5.00	mm

II.IV Setup, load cases and settings of finite-element simulation

The simulation model is created in *Ansys Workbench 2024 R2* using the *Mechanical* module from *Ansys Inc., USA*. The calculations are based on a static structural analysis of a simplified yet functionally representative simulation setup.

The surrogate specimen with the integrated spring element (a) is positioned on a cylindrical bearing (b), which replicates the biomechanical conditions on the back of the hand, specifically the joint region of the MCP-II. Fig. 4 (A) shows the complete simulation setup, while Fig. 4 (B) illustrates the anatomical analogy to the actual application in a hand orthosis.

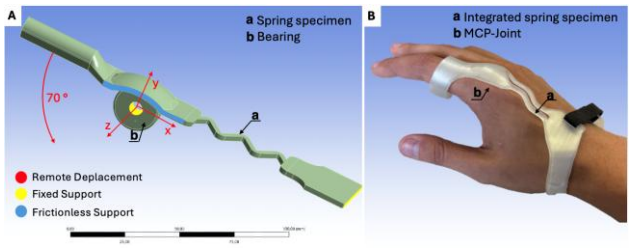

Figure 4: Simulation setup with boundary conditions (A), anatomical analogy to the simulation setup (B)

To simulate a gripping movement, for example when lifting an object, the component is rotated by 70° around the Z-axis of the bearing over a period of six seconds. The load is then maintained for 60 seconds to imitate the gripping and holding of an object. In the simulation the holding time is employed capturing the time dependent behavior and relaxation of the spring element under static loading. The temporal sequence of the simulation steps is presented in Table 3 and comprises three load steps with different time steps. During the Loading (L), a time step of 0.6 seconds is selected to minimize the computation time. The holding time is divided into two steps. The initial decrease in force during relaxation (H1) after 4.0 s, as well as the force at the end of the hold (H2).

Table 3: Load steps of the FE simulation

Nr.	Load step	Total time	Rotation	Time step
1	Loading (L)	6.0 s	70.0°	0.6 s
2	Holding (H1)	10.0 s	0.0°	4.0 s
3	Holding (H2)	66.0 s	0.0°	56.0 s

The movement is initiated via a “remote displacement” (red) applied to the lever arm of the specimen. To ensure realistic reaction force development, the opposing clamping surface of the specimen is fully constrained using a “fixed support” (yellow). The boundary conditions and support configurations are also shown in Fig. 4 (A). A frictionless contact is assumed between the cylindrical bearing and the specimen. In addition, a “frictionless support” (blue) is applied at the flanks of the recess. This prevents lateral sliding of the specimen during loading and contributes to the convergence of the simulation.

The surrogate specimen is analyzed using one of the three TNM, while the bearing is assumed to be infinitely rigid. The numerical analysis is performed with a global mesh size of 1 mm, while the area of the spring geometry is locally refined. The degree of mesh refinement was determined through a convergence analysis. Mesh sizes of 75 %, 50 %, and 25 % of the original 1 mm mesh were examined. The best compromise between simulation accuracy and computational time was found at 50 % refinement at 0.5 mm mesh size. Quadratic hexahedral elements are employed, supplemented by pyramidal elements in regions with pronounced cross-sectional changes to ensure stable meshing.

The evaluation of simulation data includes calculating the operating moment of the specimen about the bearing and the resulting tension force at the fixed clamping surface. It also involves determining the maximum strain and displacement in the spring area.

II.V Validation of finite-element simulation

The accuracy of the simulation is assessed using eleven validation points that have been specifically selected. These points correspond to the corners of the investigated parameter space, i.e. parameter sets for which all the considered factors are at their minimum or maximum values, see Fig. 5 (red). Additionally, five points along the diagonal of the parameter space are examined, where all parameters take identical levels (blue). By selecting these points, both the frame and the interior of the parameter space is validated. This implies that space can be examined almost uniformly with a minimal number of points.

Infinite Science Publishing

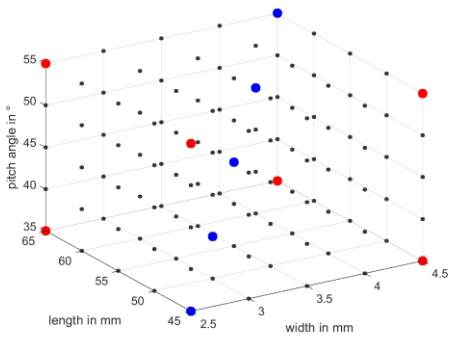

Figure 5: Validation parameter sets – points at extreme values (red), points along the bisector (blue)

For each of the eleven parameter sets, a specimen is manufactured on a *Prusa MK4*. This is carried out for the three build orientations. In total, 33 specimens are produced. The material used is identical to that utilized in the cyclic tensile tests. The manufacturing parameters also correspond to the settings documented in Table 2. For the diagonal and vertical specimens, support structures are removed during post-processing. For all orientations, the recess is subsequently post-processed by grounding to minimize friction between the support and the specimen.

Experimental data acquisition is carried out on a custom-built test rig, which allows rotation-induced deformation of the surrogate specimens (a) around a defined axis, see Fig. 6. A stepper motor is used in combination with a gearbox with 1:8 gear ratio to achieve a maximum torque of approximately 4.0 Nm. Simultaneously, the resulting tensile force F is recorded using a 100 N force transducer (b), and the operating moment M about the cylindrical bearing is measured using a 20 kgf load cell (c) at a fixed lever arm of 75 mm.

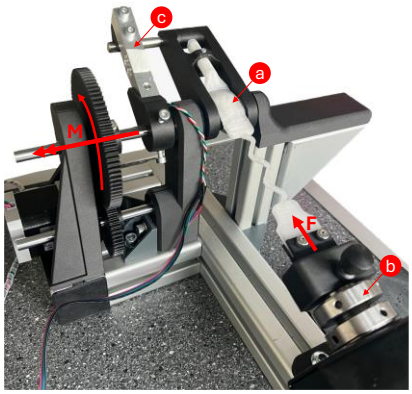

Figure 6: Test rig setup – test specimen (a), 100 N force transducer (b), 20 kgf load cell (c)

To estimate the quality of the simulation, the normalized mean absolute deviation (NMAD) between the simulation and the experiment for the target variable Y in this case, the resulting tensile force and the operating moment, is calculated, as in (1):

$$NMAD = \frac{mean(|Y_{experiment} - Y_{simulation}|)}{mean(|Y_{experiment}|)} \quad (1)$$

Due to the small sample size of n = 1 for each parameter set and manufacturing direction, it is not possible to make statistically reliable statements about the reproducibility of the experimental results. Accordingly, the standard deviation cannot be calculated. The mean absolute deviation is used, as this is less sensitive to outliers than variance- or square-based measures [20]. The simulation model of a given build orientation is therefore considered valid if the calculated NMAD across all investigated validation points averages below 15 %. While this threshold is not a universal standard, it allows for an initial qualitative assessment of the model's accuracy. As there is no universally accepted limit for 'good fit', the NMAD is also supported by a visual plausibility check.

III. Results and discussion

The following section presents the outcomes of the simulation validation in addition to the analysis of the DoE and regression models.

III.I Validation and evaluation of mechanical behavior

Validation is carried out by comparing the simulation results with experimentally obtained data from the previously defined validation parameter sets. This process is iterative: if one of the initially determined material models does not meet the specified maximum deviation of NMAD $\leq$ 15.0 %, the parameters of the corresponding TNM are adjusted and compared again with the experimental datasets.

Table 4: Validated TNMs based on build orientation

Nr.	*Symbol*	*Horizontal*	*Diagonal*	*Vertical*
1	μ_A	56.548	55.415	44.068
2	$\widehat{\Theta}$	-273.150	-273.150	-273.150
3	λL	5.100	5.100	5.100
4	κ	1153.000	1021.000	1062.000
5	$\hat{\tau}_A$	9.099	6.262	6.277
6	a	0.000	0.000	0.000
7	m_A	3.2480	4.287	3.940
8	n	0.000	0.000	0.000
9	μ_{Bi}	50.745	32.632	35.959
10	μ_{Bf}	43.971	28.526	28.138
11	β	14.648	12.279	12.793
12	$\hat{\tau}_B$	11.602	7.432	4.091
13	m_B	15.818	18.920	24.981
14	μ_C	6.008	2.107	4.097
15	q	0.000	0.000	0.000
16	α	0.000	0.000	0.000
17	Θ_0	19.850	19.850	19.850

The result of this process are three material models of validity, each representing a different type of build orientation, see Table 4. These models are then utilized to simulate all 125 parameter sets corresponding to the respective build orientation.

The greatest agreement between simulation and experiment was observed for the diagonal orientation, with a mean NMAD of 12.6 %± 9 pp over all validation points. This is followed by the horizontal orientation with 13.8 % ± 12 pp, while the model for the vertical build direction shows the largest mean NMAD of 14.3 % ± 9 pp. An exemplary comparison between simulation and experiment is presented in Fig. 7 for the characteristic parameter configuration "X-4.5-65.0-55.0" in horizontal (A), diagonal (B) and vertical (C) orientation. The curves illustrate the time-dependent evolution of force and moment from simulation and experiment. The X-axis represents time in seconds, while the Y-axis shows the tensile force in N and the operating moment in Nmm.

is realistically reproduced in both material models with a slight curvature. The deviation increases at the point of maximum loading (t = 6 s), particularly in the moment response (red) of the horizontal orientation, see Fig. 7 (A). In this instance, the simulation values exceed those of the experiment in almost all the tested parameter sets. This discrepancy can be attributed, on the one hand, to the simplified assumption of frictionless supports in the numerical model. On the other hand, effects such as friction or deformations within the test rig may also be implicated. A comparison between horizontal and diagonal orientations reveals that the maximum tensile force for identical parameter sets is consistently higher in the horizontal orientation than in the diagonal one, which indicates a higher stiffness in the horizontal orientation. The same applies to the moment.

During the subsequent holding period (H1 and H2), relaxation of the material can be observed in the experimental data. This viscoelastic behavior is captured

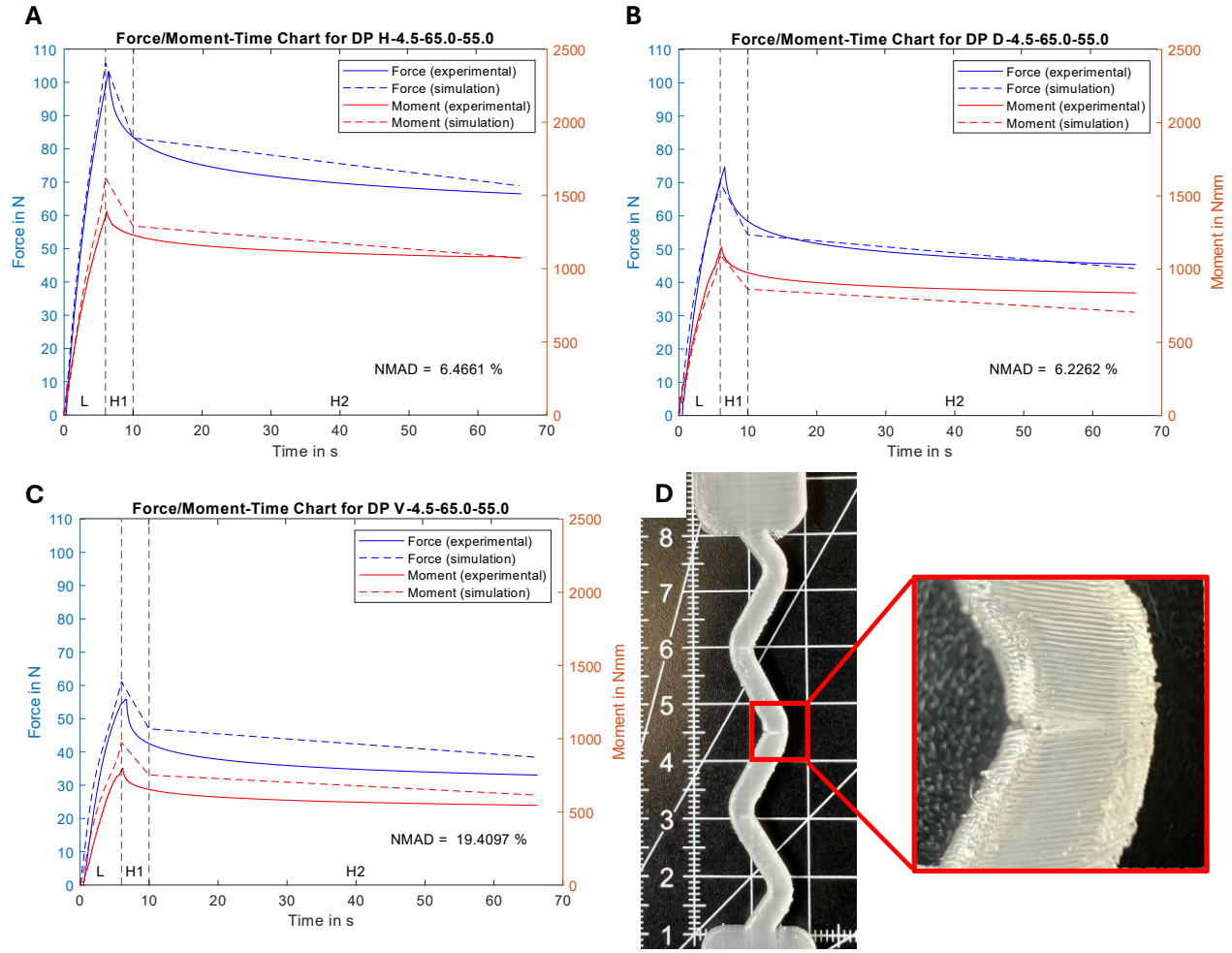

Figure 7: Force/Moment-time diagrams of the parameter set 'X-4.5-65.0-55.0' for horizontal (A), diagonal (B) and vertical orientation, (C), vertical-orientated test specimen with an interlaminar crack (D)

Firstly, the horizontal (A) and diagonal (B) orientations are considered. In both cases, generally good agreement between simulation and experiment is observed during the loading phase (L). The rise in the force and moment curves

by the TNM. However, a certain deviation becomes apparent when comparing the simulation with the experimental results, as the simulation represents the relaxation behavior in a strongly linearized form due to

large time steps. To enhance the accuracy of the numeric TNM, the material parameters, specifically the shear modulus and flow resistances of network A, B were calibrated during the validation iterations in order to ensure the accurate representation of the force at the end of the holding period. The force reduction due to relaxation is of high importance for this application. While gripping and holding objects, the resulting force on the CMC joint should not fall below a certain threshold even after an extended period, to relieve the joint.

The vertical build orientation, as shown in Fig. 7 (C), exhibits different behavior in the force/moment-time curve compared to the horizontally and diagonally manufactured variants. The maximum forces and moments occurring in the vertical orientation are even lower than the other two orientations. While the simulation and experiment agree qualitatively and quantitatively at the beginning of the loading phase (up to approximately four seconds), significant deviations occur before the end of the loading phase at t = 6 s, Fig. 7 (C). This is manifested by an abrupt change in the slope of the force and moment curve in the experiment. In contrast, the simulation shows an almost constant slope throughout this phase, similar to the horizontal and diagonal orientations. This discrepancy is due to plastic deformation and the onset of failure of the specimens. As can be seen in Fig. 7 (D), the specimen 'V-4.5-65.0-55.0' already shows pronounced damage at the end of the loading phase and is on the verge of complete failure. Other vertically manufactured samples failed completely during the experiment. Cracking always occurs in the inner radii of the spring structure between two layers. These cross-sections are most stressed. In vertically manufactured samples, the layer boundaries act as notch-like weak points due to their transverse orientation relative to the direction of loading. This means that even slight exceedance of the yield strength leads to initial crack formation, and progressive loading has a strong crack-opening effect.

The underlying TNM does not consider damage mechanisms [21]. To obtain a numerical representation of the failure behavior, the strain at maximum stress is evaluated. For this purpose, a reference value for the permissible, non-critical strain is utilized. This yield strength is determined using cyclic tensile tests conducted in accordance with the test procedure shown in Fig. 3 on an *AGS-G 10 kN* universal testing machine manufactured by *Hegewald & Pescheke GmbH, Germany*.

The resulting strain is captured with *ARAMIS* the optical measurement system from *Carl Zeiss Gom Metrology GmbH, Germany*. Figure 8 illustrates the stress-strain diagram for characteristic horizontal (red), diagonal (green) and vertical (blue) standardized tensile test specimens. The yield strain (circled) is 0.18 ± 0.03 for the horizontal orientation, 0.16 ± 0.05 for the diagonal orientation, and 0.15 ± 0.04 for the vertical orientation. These limits are used to detect material and layer orientation specific failure due to overload in the post-processing of the simulation data. Overall, the evaluation shows that samples manufactured vertically have lower load-bearing capacity and lower strain at yield than those manufactured horizontally or diagonally.

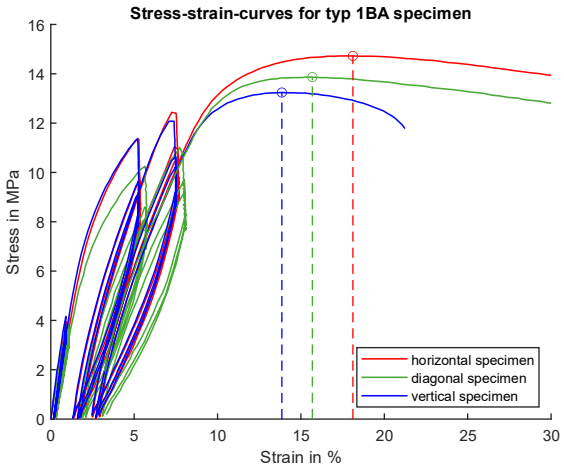

Figure 8: Stress-strain diagram – cyclic tensile tests with standardized specimens in horizontal (red), diagonal (green) and vertical (red) build orientation

III.II Analysis of the mathematical model, parameters and interactions

The resulting data from the simulations will be used to determine the influence of the geometric parameters (width, length and pitch angle) and the manufacturing parameter (build orientation) on three target variables. These targets are the tensile force, the operating moment and the spring elongation.

For the quantitative analysis of these influences, a quadratic regression model with 14 coefficients according to (2) is used.

$$\begin{aligned} Y = {} & \beta_0 + \beta_1 \cdot \text{orientation} + \beta_2 \cdot \text{width} \\ & + \beta_3 \cdot \text{length} \\ & + \beta_4 \cdot \text{angle} \\ & + \beta_5 \cdot (\text{orientation} \cdot \text{width}) \\ & + \beta_6 \cdot (\text{orientation} \cdot \text{length}) \\ & + \beta_7 \cdot (\text{orientation} \cdot \text{angle}) \\ & + \beta_8 \cdot (\text{width} \cdot \text{length}) \\ & + \beta_9 \cdot (\text{width} \cdot \text{angle}) \\ & + \beta_{10} \cdot (\text{length} \cdot \text{angle}) \\ & + \beta_{11} \cdot \text{width}^2 \\ & + \beta_{12} \cdot length^2 + \beta_{13} \cdot angle^2 \end{aligned} \tag{2}$$

This formula considers the three geometric factors, as well as the orientation, which is treated as a categorical factor. The orientation is incorporated using dummy coding. The horizontal orientation serves as the reference category. In addition to the linear and quadratic terms, as well as the interactions between the numerical factors, interaction terms between the numerical factors and the categorical factor are included. This enables the mapping of direction-dependent effect patterns of individual geometric

parameters. The regression model was created and analyzed using *MATLAB R2024b by The MathWorks Inc., USA.*

Three distinct calculation models were derived from the regression analysis. These models achieve a good agreement, with a coefficient of determination (R^2) of 99.8 % for the tensile force, 99.7 % for the operating moment and 98.4 % for the spring elongation.

In the designated parameter space, with 125 parameter sets for each build orientation, the implementation of these calculation models enables the prediction of the target variables. The mean absolute error for tensile force is 1.2 N, for operating moment 18.5 Nmm, and for elongation 0.04, compared to the results of the FE simulation of those parameter sets.

As presented in Table 5, the regression coefficients of the model and their standard deviation are utilized to predict the three target variables. All terms of the three regression models fall below the predetermined significance level of $\alpha = 0.05$, with most of them exhibiting clear statistical significance. The linear factor of the pitch angle (marked red), when used to predict the tensile force, is the only factor to exceed this threshold. However, it is essential to acknowledge the significance of the interactions between the pitch angle and the other factors, as well as the quadratic interaction with itself. For reasons pertaining to the hierarchical structure of the model, the linear factor is retained and not eliminated due to its lack of significance. The effect of the influencing factors can be assessed based on the signs and values of the regression coefficients. For all three calculation models, the influences of the four main parameters are similarly oriented but differ in their magnitude. The variation in orientation from horizontal to diagonal or vertical, as well as the increase in width and pitch angle, lead to an increase in the respective target variable. Conversely, an increase in length results in a decline in the target variable.

The low values of the interaction terms indicate a generally weak mutual influence of the parameters. The quadratic terms also have coefficients of low magnitude. Whilst exhibiting a weak curvature, these elements contribute substantially to the optimization of the mathematical model. This observation serves to reiterate the nonlinear behavior of the PP.

Table 5: Coefficients of the quadratic regression model with dummy variables β_5-β_7 for the target variables: tensile force, operating moment and elongation

	Tensile force	***Operating moment***	***Spring elongation***
β_0	-2.044E+01 ± 7.324E+00	-2.665E+02 ± 1.104E+02	2.263E+00 ± 2.183E-01
β_{1D}	2.796E+01 ± 1.744E+00	3.141E+02 ± 2.630E+01	1.752E-01 ± 5.199E-02
β_{1V}	3.727E+01 ± 1.744E+00	4.276E+02 ± 2.630E+01	1.094E-01 ± 5.199E-02
β_2	1.495E+00 ± 1.399E-01	2.918E+01 ± 2.109E+00	6.134E-02 ± 4.169E-03
β_3	-7.782E-01 ± 1.821E-01	-1.557E+01 ± 2.747E+00	-1.332E-01 ± 5.428E-03
β_4	**2.065E-03 ± 1.600E-02**	8.412E-01 ± 2.413E-01	5.725E-03 ± 4.770E-04
β_{5D}	-9.768E-01 ± 2.193E-02	-1.302E+01 ± 3.308E-01	2.851E-03 ± 6.537E-04
β_{5V}	-1.165E+00 ± 2.193E-02	-1.567E+01 ± 3.308E-01	-1.413E-03 ± 6.537E-04
β_{6D}	5.438E-01 ± 2.193E-02	6.952E+00 ± 3.308E-01	-6.057E-03 ± 6.537E-04
β_{6V}	5.582E-01 ± 2.193E-02	7.614E+00 ± 3.308E-01	1.445E-03 ± 6.537E-04
β_{7D}	-1.001E-01 ± 2.193E-03	-1.286E+00 ± 3.308E-02	3.503E-04 ± 6.537E-05
β_{7V}	-1.183E-01 ± 2.193E-03	-1.578E+00 ± 3.308E-02	-1.826E-04 ± 6.537E-05
β_8	-2.653E-02 ± 1.266E-03	-3.151E-01 ± 1.910E-02	-6.618E-04 ± 3.774E-05
β_9	2.659E-03 ± 1.266E-04	2.312E-02 ± 1.910E-03	-1.959E-05 ± 3.774E-06
β_{10}	-1.729E-03 ± 1.266E-04	-2.184E-02 ± 1.910E-03	-8.825E-06 ± 3.774E-06
β_{11}	2.004E-02 ± 1.514E-03	2.001E-01 ± 2.282E-02	-5.250E-05 ± 4.511E-05
β_{12}	1.118E-02 ± 1.514E-03	1.728E-01 ± 2.282E-02	1.173E-03 ± 4.511E-05
β_{13}	3.100E-04 ± 1.514E-05	3.711E-03 ± 2.282E-04	-3.450E-06 ± 4.511E-07

In comparison with a linear regression model, a significant decrease in mean absolute error is observed in the quadratic models. Regarding the error in tensile force between the regression model and the simulated parameter space, the mean error is reduced by approximately fivefold when a quadratic model (1.2 N) is employed in comparison with a linear model (6.2 N). To investigate whether the quadratic extension enhances predictive capability or results in

overfitting and increases model complexity, a residual analysis is performed.

This involves plotting the difference between the measured response and the model prediction against the fitted values. Figure 9 presents the plots of the residual analysis for the linear model (A) and the quadratic model (B). This representation enables the identification of systematic deviations and thus reveals potential model misspecification.

For the linear model (A), the residuals exhibit a pronounced systematic curvature in the form of a U-shaped pattern. A linear approach enforces a constant slope over the entire domain and is therefore unable to represent an underlying nonlinear relationship with curvature. As a result, the model consistently underestimates the response in one part of the input space and overestimates it in another. This alternating bias is evident in the structured residual distribution, indicating the relevance of higher order terms.

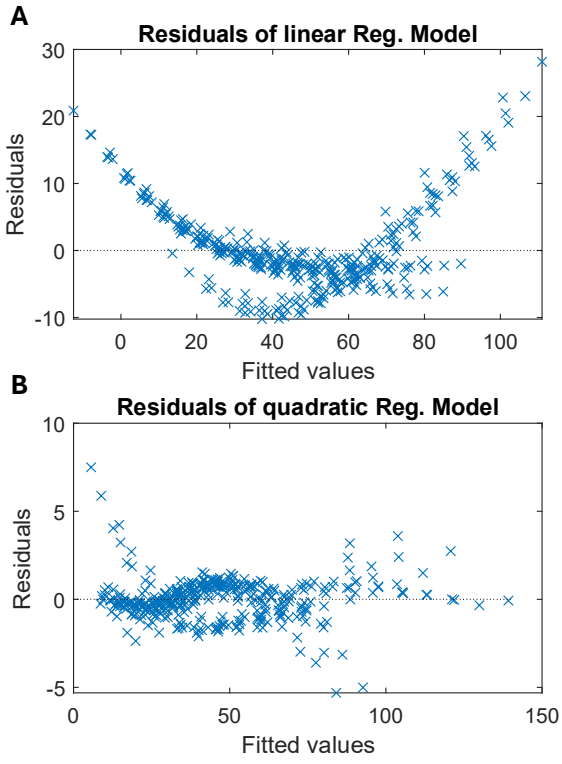

Figure 9: Residual analysis of the linear (A) and the quadratic (B) regression model

In contrast, the quadratic model explicitly incorporates two-way interactions and second order terms, allowing the representation of curvature in the input output relationship. As a result, the systematic component of the deviation is captured by the model itself rather than remaining in the residuals. Accordingly, the residuals in (B) do not exhibit any recognizable pattern and are mostly random scattered around the zero line. The disappearance of the structured U-shaped pattern, combined with the random distribution of residuals, demonstrates that the quadratic model provides a structurally adequate description of the data and therefore represents a justified extension of the linear approach.

The experimental data can be used to determine the total error, consisting of the deviation of the simulation and subsequent mathematical modelling. The resulting errors are 8 % for the prediction of tensile force and 14 % for the operating moment. The limitations of this approach become evident when analyzing the operating moment prediction error. The magnitude of this error is almost double that of the tensile force. This phenomenon can be attributed to unaccounted friction and elastic deformations within the test rig. The overall system deviates by a total of 11 %. The total error is moderate and within an acceptable range for qualitative assessments of the mechanical system response. To achieve precise quantitative predictions, it is essential to incorporate physical influences such as friction into the simulation model. Furthermore, experimental uncertainties, including those arising from deformations in the test setup e.g. slippage in the gear box or measuring errors, should be minimized to enhance accuracy.

Additionally, it is crucial to emphasize that the model predictions and their accuracy are only valid within the parameter space covered. Extrapolation outside this range is associated with increased uncertainty.

III.III Selection of spring geometries based on patient-specific biomechanical requirements

The mathematical models obtained from the quadratic regression analysis can be used to predict the target values for any combination of the four input parameters within the validated parameter space. To adapt the spring geometry to the biomechanical requirements of the respective patient, it is necessary to solve the inverse problem. Rather than deriving forces and moments from established geometric parameters, these geometric parameters are determined based on defined biomechanical parameters.

The width and pitch angle of the spring are identified as the geometric parameters to be determined, as these cannot be derived from individual patient data. The other parameters including the length, operating moment and tensile force, are derived from patient-specific characteristics and are specified accordingly. The characteristics are based on the length of the back of the hand, the maximum grip strength of the index finger, which corresponds to the moment exerted on the MCP-II joint, and the force required to spread the CMC joint. The elongation originally defined as a target value is used as an exclusion criterion for a configuration. If a parameter set exceeds the specified yield strain limit for the respective build orientation (Fig. 8), it is excluded due to probable failure.

To put this principle into practice, a user interface is being developed that allows patient-specific characteristics to be

entered, see Fig. 10. The optimal geometric parameters will be output by the design tool once the individual parameters have been entered. These individual parameters are back of hand length, grip strength and the required spreading force. The range between the minimum and maximum spreading force results in several combinations of parameter configurations that equally meet the biomechanical requirements. Additionally, the configuration that offers the best overall balance of manufacturing efficiency and stability reserves can be output (shown green).

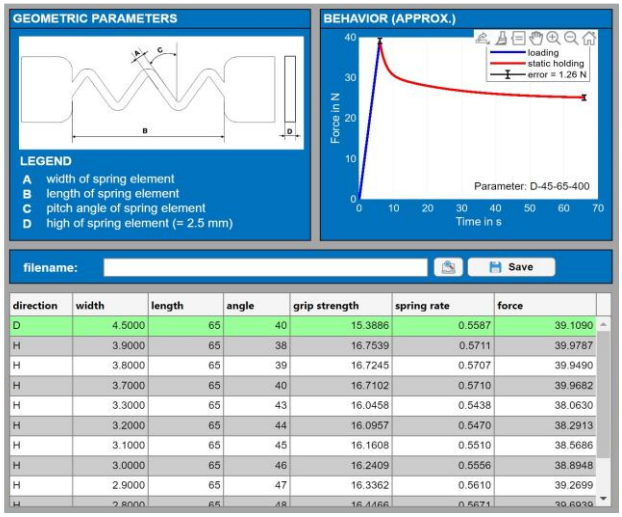

direction	width	length	angle	grip strength	spring rate	force
D	4.5000	65	40	15.3886	0.5587	39.1090
H	3.9000	65	38	16.7539	0.5711	39.9787
H	3.8000	65	39	16.7245	0.5707	39.9490
H	3.7000	65	40	16.7102	0.5710	39.9682
H	3.3000	65	43	16.0458	0.5438	38.0630
H	3.2000	65	44	16.0957	0.5470	38.2913
H	3.1000	65	45	16.1608	0.5510	38.5686
H	3.0000	65	46	16.2409	0.5556	38.8948
H	2.9000	65	47	16.3362	0.5610	39.2699

Figure 10: Design tool with patient-specific parameters

A total of twelve valid geometry variants were identified using the developed methodology in an exemplary case. Of these, the 'D-4.5-65.0-40.0' parameter set was chosen. This set offers the most favorable ratio of mechanical properties to material usage and post-processing time. The diagonal orientation enables the entire orthosis to be positioned material efficient within the build space of the FFF printer. The spring geometry shown in Fig. 11 (red) was adapted to the requirements of a test subject and integrated into a design draft for a hand orthosis for the treatment of carpometacarpal osteoarthritis.

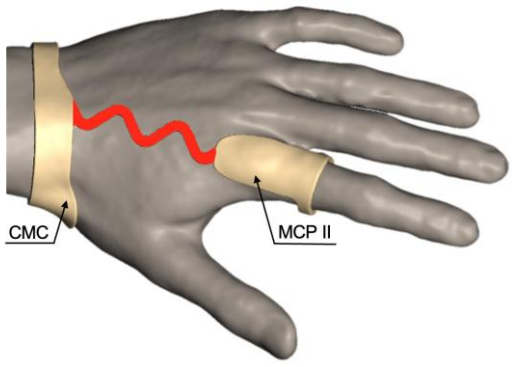

Figure 11: Design draft of a hand orthosis with an individually adapted spring element (red)

IV. Conclusion

This study demonstrates that a parameterized simulation model can be used systematically to predict the mechanical behavior of functional orthotic components. Using the Three-Network-Model has proven to be an effective way of mapping the complex, nonlinear deformation behavior of additively manufactured polypropylene.

A high degree of agreement was observed between the simulation and experiment for the diagonal and horizontal manufacturing orientations. The normalized mean absolute deviations (NMAD) of 12.6 % and 13.8 %, respectively, are both found to be within the predefined tolerance range. However, due to the limited sample size (n = 1) in the validation process, it was not possible to perform a quantitatively optimal calibration of the material models for the finite element method. In view of the time and resource constraints, only one specimen was manufactured for each parameter combination and orientation for validation purposes. Therefore, it is not possible to make any statements about the dispersion or reproducibility of the measurement results.

This limited statistical significance accounts for the majority of the total error in this work. It has been observed that the vertical manufacturing orientation is representative of the limits of the simulation model and the material's load-bearing capacity.

The samples that were manufactured vertically for the experimental validation exhibited signs of plastic deformation or complete failure. This highlights the necessity to establish a criterion for the maximum permissible load limit in the simulation or in the post processing of the simulation data, to identify cases of failure in advance and immediately exclude affected parameter sets. In this context, strain or stress-based failure criteria should be employed to ensure that the increase in model complexity remains proportionate to the enhancement in predicting possible failure.

The regression models developed to map the relations between geometric and manufacturing parameters and target variables demonstrate a high predictive accuracy of $R^2 \geq 99.7$ % for tensile force and operating moment, and $R^2 \geq 98.4$ % for maximum elongation of the spring element. The integration of linear main effects, two-way interactions and quadratic terms allows for the precise modelling of the behavior between parameters.

The high statistical significance of the quadratic and interactive terms between two parameters is particularly noteworthy, emphasizing the importance of nonlinear terms in modelling the system. Assuming a linear model, the mean absolute errors of the target variables would increase by a factor of five. This finding indicates that the target variables cannot be adequately described solely by the main effects of the individual parameters. Instead, these variables are also significantly determined by their mutual interactions and by nonlinear amplification effects. In addition to the uncertain reproducibility of simulation validation, the neglect of tribological and rheological

effects, as well as the deviations resulting from regression analysis, contribute to the total error. The total error can currently only be estimated from 33 experimental data sets and averages 11 %. However, the tension over time can be mapped with a deviation of 8 %, as opposed to the operating moment, which exhibits a deviation of 14 %. The findings of this research demonstrate that simulationbased design methodology possesses significant potential for the development of customized, additively manufactured orthotic components. Future research efforts should focus on extending the model by incorporating larger validation datasets, with the aim of including tribological and rheological effects. Additionally, integrating the model into practical software tools should be prioritized to facilitate its translation into orthopedic care.

Acknowledgments

The authors would like to express their gratitude to Hochschule Stralsund for its comprehensive support in conducting this research. Further they like to express their appreciation to TBI-MV GmbH for funding the project. (TBI-1-155-W-047) The financial support facilitated the execution of experimental investigations and associated analyses.

Author's statement

Conflict of interest: The authors declare no conflicting interests. Informed consent: Informed consent has been obtained from all individuals included in this study. Ethical approval: The research related to human use complies with all the relevant national regulations, institutional policies and was performed in accordance with the tenets of the Helsinki Declaration, and has been approved by the authors' institutional review board or equivalent committee.

References

[1] W. Bureck, A. Kark, I. Gundelwein, H. Wendt, M. Behrendt, and M. Langer, *Schienenversorgung in der Handtherapie: Bauanleitungen für statische, dynamische und statisch-progressive Schienen*. Berlin, Heidelberg: Springer Berlin Heidelberg, 2020. doi: 10.1007/978-3-662-53788-6.

[2] 'Orthopädische Geräte - Deutschland | Statista Marktprognose', Statista. Accessed: Jun. 16, 2025. [Online]. Available: http://frontend.xmo.prod.aws.statista.com/outlook/hmo/medizintechnik/medizinische-geraete/orthopaedische-geraete/deutschland

[3] Ł. Jaworski and R. Karpiński, 'BIOMECHANICS OF THE HUMAN HAND', *J. Technol. Exploit. Mech. Eng.*, vol. 3, no. 1, pp. 28–33, Jun. 2017, doi: 10.35784/jteme.536.

[4] F. Kerkhof, D. Kenney, M. Ogle, T. Shelby, and A. Ladd, 'The biomechanics of osteoarthritis in the hand: Implications and prospects for hand therapy', *J. Hand Ther.*, vol. 35, no. 3, pp. 367–376, Jul. 2022, doi: 10.1016/j.jht.2022.11.007.

[5] S. L. S. Houwen-van Opstal, Y. M. E. M. Van Den Elzen, M. Jansen, M. A. A. P. Willemsen, E. H. C. Cup, and I. J. M. De Groot, 'Facilitators and Barriers to Wearing Hand Orthoses by Adults with Duchenne Muscular Dystrophy: A Mixed Methods Study Design', *J. Neuromuscul. Dis.*, vol. 7, no. 4, pp. 467–475, Sep. 2020, doi: 10.3233/JND-200506.

[6] T. Oud, J. A. Bogaards, F. Nollet, and M.-A. Brehm, 'Preliminary effectiveness and production time and costs of three-dimensional printed orthoses in chronic hand conditions: an interventional feasibility study', *J. Rehabil. Med.*, vol. 56, p. jrm39946, May 2024, doi: 10.2340/jrm.v56.39946.

[7] O. Ciobanu and G. Ciobanu, 'THE USE OF 3D SCANNING AND RAPID PROTOTYPING IN MEDICAL ENGINEERING', *Fiabil. Şi Durabilitate*, vol. 1-supl, pp. 241–247, May 2013.

[8] S. Logozzo, E. M. Zanetti, G. Franceschini, A. Kilpelä, and A. Mäkynen, 'Recent advances in dental optics – Part I: 3D intraoral scanners for restorative dentistry', *Opt. Lasers Eng.*, vol. 54, pp. 203–221, Mar. 2014, doi: 10.1016/j.optlaseng.2013.07.017.

[9] A. Cirello *et al.*, 'A New Automatic Process Based on Generative Design for CAD Modeling and Manufacturing of Customized Orthosis', *Appl. Sci.*, vol. 14, no. 14, Art. no. 14, Jan. 2024, doi: 10.3390/app14146231.

[10] F. Pfeiffer, 'The Use of Finite Element Analysis to Enhance Research and Clinical Practice in Orthopedics', *J. Knee Surg.*, vol. 29, no. 02, pp. 149–158, Jan. 2016, doi: 10.1055/s-0035-1570114.

[11] C. B. Park and H.-S. Park, 'Portable 3D-printed hand orthosis with spatial stiffness distribution personalized for assisting grasping in daily living', *Front. Bioeng. Biotechnol.*, vol. 11, Feb. 2023, doi: 10.3389/fbioe.2023.895745.

[12] S. Lierde, 'Latest medical applications of polypropylene', *Med. Device Technol.*, vol. 15, pp. 33–4, Jul. 2004.

[13] K. Siebertz, D. Van Bebber, and T. Hochkirchen, *Statistische Versuchsplanung*. Berlin, Heidelberg: Springer, 2017. doi: 10.1007/978-3-662-55743-3.

[14] S. V. Gohil, S. Suhail, J. Rose, T. Vella, and L. S. Nair, 'Chapter 8 - Polymers and Composites for Orthopedic Applications', in *Materials for Bone Disorders*, S. Bose and A. Bandyopadhyay, Eds, Academic Press, 2017, pp. 349–403. doi: 10.1016/B978-0-12-802792-9.00008-2.

[15] 'P-filament 721 natural | PPprint'. Accessed: Jun. 10, 2025. [Online]. Available: https://www.ppprint.de/produkt/filament/

[16] V. Delbruel, A. Banoune, N. Tardif, J. Duchet-Rumeau, T. Elguedj, and J. Chevalier, 'Quantifying the effect of material stiffness and wall thickness on the mechanical properties of ankle–foot orthoses manufactured by material extrusion', *Prog. Addit. Manuf.*, vol. 10, no. 2, pp. 1447–1459, Feb. 2025, doi: 10.1007/s40964-024-00717-7.

[17] J. Bergstrom, 'PolyUMod - A Library of Advanced User Materials V.4.5.0'. Veryst Engineering LLC., Needham MA, 2015.

[18] M. Jin, C. Neuber, and H.-W. Schmidt, 'Tailoring polypropylene for extrusion-based additive manufacturing', *Addit. Manuf.*, vol. 33, p. 101101, May 2020, doi: 10.1016/j.addma.2020.101101.

[19] T. Haupt, 'Analyse der Kennwerte eines Federelements einer additiv gefertigten Orthese: Simulation und optische Messung im Vergleich', Bachelorarbeit, Maschinenbau, Stralsund, 2023.

[20] T. O. Hodson, 'Root-mean-square error (RMSE) or mean absolute error (MAE): when to use them or not', *Geosci. Model Dev.*, vol. 15, no. 14, pp. 5481–5487, Jul. 2022, doi: 10.5194/gmd-15-5481-2022.

[21] J. S. Bergstrom and J. E. Bischo, 'An Advanced Thermomechanical Constitutive Model for UHMWPE', 2010.